Study of concrete damage mechanism under hydrostatic pressure by numerical simulations

Jian Cui, Hong Hao* and Yanchao Shi

Tianjin University-Curtin University Joint Research Centre of Structure Monitoring and Protection

School of Civil Engineering, Tianjin University, China

School of Civil and Mechanical Engineering, Curtin University, Australia

Abstract: Current material models commonly assume concrete does not suffer damage under hydrostatic pressure. However concrete damages were observed in recent true tri-axial tests. Hydrostatic pressures varying from 30 MPa to 500 MPa were applied on the 50 mm cubic concrete specimens in the tests. Uniaxial compressive tests and microscopic observations on the hydrostatic tested specimens indicated that concrete suffered obvious damage if the applied hydrostatic pressure was higher than the uniaxial compressive strength of concrete specimen. This study aims to examine damage mechanism of concrete under hydrostatic pressures through numerical simulations. A mesoscale concrete model with the consideration of randomly distributed aggregates and pores is developed and verified against the testing data, and then used to simulate the responses of concrete specimens subjected to different levels of hydrostatic pressures. The simulation results show that under hydrostatic pressure there are significant deviatoric stresses distributed inside the specimen especially in the zones around the pores and between aggregates and mortar because of the inhomogeneous and anisotropic characteristics of the concrete material. The mortar paste matrix in these zones is seriously damaged leading to concrete damage associated with significant stiffness and strength losses. More accurate concrete material models need be developed to take into consideration the damages that could be induced by hydrostatic stress.

* Corresponding author: hong.hao@curtin.edu.au (Hong Hao)

Keywords: EOS of concrete; hydrostatic pressure; mesoscale model; damage; true tri-axial test.

1. Introduction

This study focuses on the behavior of concrete subjected to hydrostatic pressures (equation of state, EOS). When a concrete structure subjects to extreme loading conditions such as near-field detonations and projectile penetrations, the material experiences a complex stress state, e.g. very high confining pressure or very high hydro pressure caused by the lateral inertial confinement. Therefore material models able to capture the behavior of concrete under complex stress-states are needed for reliable predictions of concrete structure responses to these extreme loadings. Current material models commonly assume concrete material does not suffer damage under hydrostatic pressures. In other words, no matter how high is the hydrostatic pressure applied to concrete material, it does not experience stiffness and strength loss although it suffers plastic deformation, i.e., compaction of the pores. This assumption could be true if concrete material is homogeneous and isotropic. In reality, concrete is a composite material, consisting of randomly distributed aggregates and pores in mortar matrix, and therefore is neither homogeneous nor isotropic. The assumption that hydrostatic pressure does not damage concrete material is thus not necessarily valid. To model the multiphase property of concrete material, Karinski et al. [1] developed a multi-scale mix based equation of state for cementitious materials that considers the microstructure of cement paste and concrete. In the model, cement paste represents the non-linear elastic-plastic behavior while fine and coarse aggregates are assumed to be linear elastic. The model validation shows good agreement with available test results.

Concrete is one of the most widely used construction materials in the field of civil engineering and military engineering. Thus concrete structures might be exposed to extreme dynamic loading conditions. Understanding its material behavior under complex stress-states is essential for reliable predictions of the responses of concrete structures. Most experimental results available in the literature only address the damage and destruction of concrete material under deviatoric stress [2-6], usually obtained with a cylindrical specimen subjected to an axial loading with confining pressure. Because of the lack of understanding and data to characterize the performance under hydrostatic pressures, the commonly used concrete material models in hydrocodes such as KCC model [7] and RHT model [8] in LSDYNA [9] do not consider the damage of material in hydrostatic pressure. The study of concrete under high hydrostatic pressure is limited owing to the difficulty in applying the very high true tri-axial pressures in tests. However, the damage of concrete under high hydrostatic pressure influences the failure surface, damage evolution algorithm and equation of state (EOS) of the concrete constitutive model under the complex stress states [10]. Poinard, et al [11] did a series of pseudo tri-axial tests using cylindrical concrete specimens which have a 29 MPa uniaxial compressive strength. In their research it was observed that the bulk modulus of the concrete decreased substantially after the specimen having been subjected to a hydrostatic pressure higher than 60MPa. The authors attributed this drop to cement matrix damage. Pham et al. [12] found that in their FRP-confined concrete tests, the core concrete has suffered serious damage although the FRP-confinement could significantly increase the concrete strength. Karinski et al. [13] developed an experimental setup to perform confined compression tests of cementitious material specimens at high pressures. They found that cracks occurred in specimens with W/C = 0.50 (water/cement ratio). In the other specimens made with a lower w/c ratio, no crack was observed. The authors attributed this observation to the fact that cement paste with W/C = 0.50 has higher porosity and larger maximum capillary pore size as compared to lower w/c ratios, which made the specimen more vulnerable to confined compressive loadings.

There are several approaches in numerical simulation to study concrete material behavior, i.e., macro-level, meso-level and micro-level. At macro-level, the concrete is regarded as a homogeneous material, therefore the model at this level cannot considerate the influences of individual components in concrete material on its mechanical properties. At mesoscale, the coarse aggregates, mortar matrix, pores and the interfacial transition zone (ITZ) can be modelled in detail. The computational effort of meso-level modelling is substantially higher than the macro-level model, but the influences of each component on concrete material performance can be captured. At micro-level, the mortar matrix of the previous level is further subdivided into fine aggregates and hardened cement paste. Among these levels, mesoscopic level analysis is the most practicable and it can provide more insights to the mechanical response of concrete because the volume fractions and distributions of multiple phases such as aggregates, mortar and pores can be explicitly modeled in detail. Many mesoscale concrete models [14-18] have been developed to study the anisotropic and heterogeneous behavior of concrete under different stress states. In a mesoscale model, the influence of important parameters, such as the shape, distribution and size of course aggregates within the mortar matrix are studied by different researchers [19-22]. In the study by Kim et al [20], it was concluded that aggregate shape had a weak effect on the ultimate tensile strength of concrete and on the tensile stress-strain curve. However, due to the stress concentration at the sharp edges of polygonal aggregate shape, the ultimate tensile strength of the circular shaped aggregate model was a little higher than those of the other aggregate shapes. Some previous numerical studies proved that models with circular or spherical aggregates yield reliable predictions of response of concrete specimens under different loadings [23, 24]. It should be noted that most previous studies do not consider pores although concrete material usually has an approximately 10% porosity depending on the W/C ratio [11, 25, 26].

The present study develops a three-dimensional mesoscale model of concrete with consideration of mortar matrix and randomly distributed course aggregates and pores to investigate the stress distribution inside the concrete specimen and the damage evolution due to deviatoric stresses. The commercial software LS-DYNA is employed to perform the numerical simulations. The accuracy of the numerical model is verified by testing data. The numerical model is then used to simulate concrete material responses under different levels of hydrostatic pressures to examine the behavior and the damage mechanism of concrete under high hydrostatic pressures. The results are used to analyze and explain the observed concrete material damage under hydrostatic pressures.

2. Experimental study of concrete damage under hydrostatic pressure

A series of true tri-axial tests were carried out to study the damage of concrete under high hydrostatic pressures [27]. Some representative testing data are used to verify the numerical model developed in the present study. For completeness the tests are briefly described here.

2.1 Test set-up

The experiments were conducted by a true tri-axial hydraulic servo-controlled test system developed by Central South University in China [28, 29]. The machine could apply quasi-static loads along the three principal stress directions through hydraulically driven pistons, independently. In this test, the cross section of steel load transfer block is 47 mm × 47 mm, 3 mm shorter than the 50 mm cubic specimen to avoid the collision of the load transfer bars along different directions when the specimen experiences a large strain during the loading process, as illustrated in **Fig. 1**. The axial loads was recorded by the load cell sandwiched between the actuator of the machine and the spherical hinge (**Fig. 1(a)**), and the deformation of the specimen was measured by LVDT sensors. The elastic deformation of the load transfer bar was measured by strain gauges and removed from the record of LVDT in the subsequent data analyses to obtain the strain of the tested specimen, as detailed in **Fig. 1(b)**. At the time of hydrostatic testing, the uniaxial compressive strength of concrete was also tested as 35.2 MPa on average.

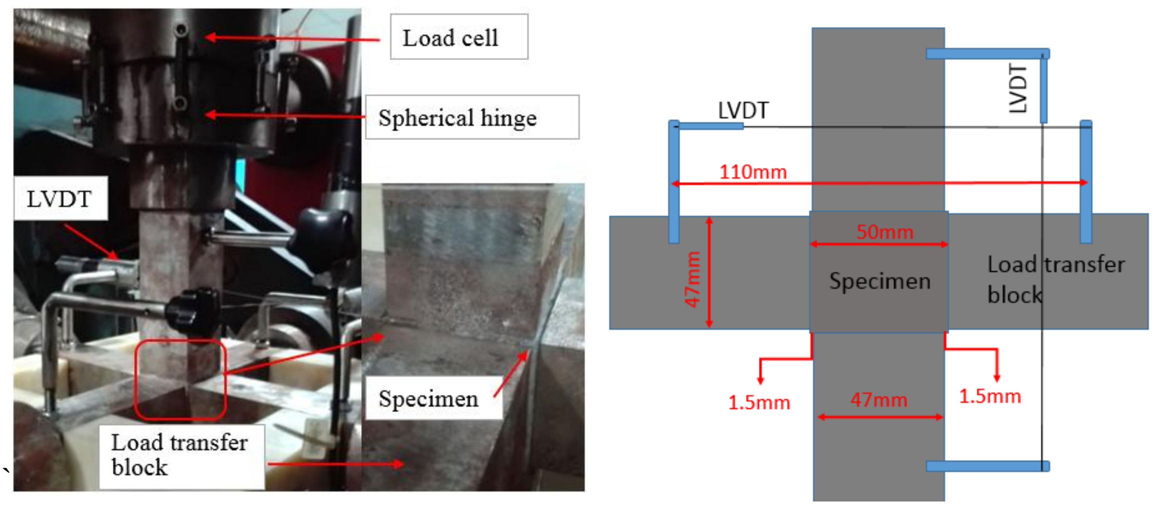

(a) (b)

Fig. 1 The test set-up: (a) overall view; (b) 2D section view

2.2 Test procedure and results

One loading-unloading cycle was applied on the cubic specimen during the hydrostatic test. To ensure $\sigma_1 = \sigma_2 = \sigma_3$ (σ_1, σ_2, and σ_3 are major, intermediate, and minor principal stresses, respectively) during the loading-unloading process, the forces of X, Y and Z axes were applied by the force control mode at a rate of 1 kN/s (0.4 MPa/s) until reaching the desired stress level. Before unloading, the desired stress level was maintained for about 6 minutes. To investigate the damage of the specimens at different levels of hydrostatic pressures, five levels of hydrostatic pressures (35 MPa, 70 MPa, 175 MPa, 350 MPa and 500 MPa) were applied on the specimen.

After hydrostatic tests, the specimen was taken out from the true tri-axial test facility and uniaxial compressive strength tests were carried out to evaluate the residual compressive strength of the tested specimens. **Fig. 2** shows the typical stress-strain curves of the tested concrete specimens under the uniaxial compression. From the figure, it is clear that as the preloaded hydrostatic pressure increases, the residual strength and Young's modulus of the concrete decrease, indicating application of hydrostatic pressure has caused damage to the concrete specimens.

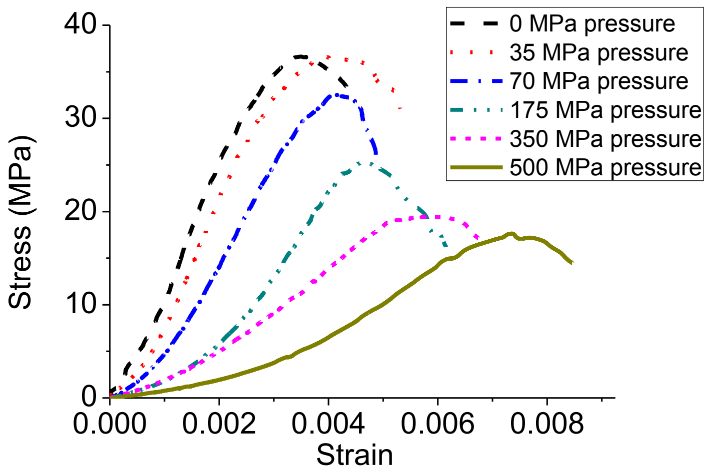

Fig. 2 Compressive stress-strain curve of the specimen after hydrostatic tests

Electron microscope provides a direct observation of the damages of the tested specimens, and hence helps to better understand the damage mechanism of concrete subjected to hydrostatic pressure. In the test, typical virgin specimens and the specimens after the application of 500 MPa were examined with an Environment Scanning Electron Microscopy (ESEM) at low vacuum mode. The typical micrographs of concrete are shown in **Fig. 3**. In the mesoscale analysis, the cement matrix/aggregate interface, also called the interfacial transition zone (ITZ) is considered to be the weakest link inside the concrete and have a significant influence on the failure mode and the macro-mechanical properties of concrete [30, 31]. The test results also confirm this conclusion. From **Fig. 3** one can find that most of the damaged areas are on the ITZ or in the cement matrix near the ITZ. The micro-cracks between the cement matrix and the course aggregates are very clear.

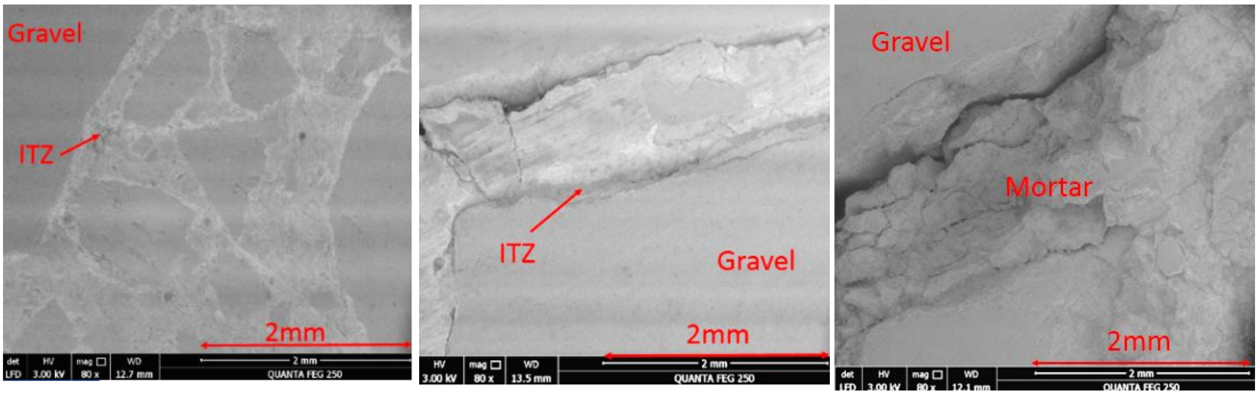

(a) (b) (c)

Fig. 3 Electron microscope photos: (a) virgin concrete; (b) and (c) concrete after application of 500 MPa hydrostatic pressure

3. 3D concrete mesoscale model

To analyze the damage that could be caused by hydrostatic pressure in more detail, a 3D mesoscale model is developed in this study to simulate the true tri-axial tests of the concrete specimens.

3.1 Material model

The plastic-damage model for concrete in LS-DYNA developed by Malvar et al [7] (Mat_072R3) is adopted to model the mortar and aggregates in the simulation [23]. This model uses three fixed shear failure surfaces with the consideration of damage and strain rate effects.

Three independent strength surfaces are an initial yield surface (F_y), a maximum failure surface (F_m) and a residual surface (F_r) with consideration of all the three stress invariants (I_1, J_2, J_3). The failure surface of hardening stage is derived by interpolating between the initial yield surface and the maximum failure surface, as is shown in Eq. (1). The failure surface of softening stage is derived by interpolating between the maximum failure surface and the residual surface, as is shown in Eq. (2). **Fig. 4** shows the three failure surfaces.

$$F\left(p, J_2, J_3, \lambda\right) = \eta(\lambda) \cdot (F_m - F_y) + F_y, \text{ for } \lambda \leq \lambda_{\mathrm{m}} \quad (1)$$

$$F\left(p, J_2, J_3, \lambda\right) = \eta(\lambda) \cdot (F_m - F_r) + F_r, \text{ for } \lambda > \lambda_{\mathrm{m}} \quad (2)$$

In Eqs. (1-2),

$$F_i\left(p, J_2, J_3\right) = \Delta\sigma_{\mathrm{i}}^{\mathrm{c}} \times r' \qquad \text{i=m, y or r} \quad (3)$$

where $\Delta\sigma_{\mathrm{i}}^{\mathrm{c}}$ represents the compressive meridians of the three independent strength surfaces:

$$\Delta\sigma_{\mathrm{i}}^{\mathrm{c}} = a_{0\mathrm{i}} + \frac{p}{a_{1\mathrm{i}} + a_{2\mathrm{i}} \cdot p} \quad (4)$$

in which parameters a_{0i}, a_{1i}, a_{2i} need to be determined from test data. r' is an implementation of the William and Warnke equation [32] to consider the influence of the second stress invariants J_2.

λ is the modified effective plastic strain or the damage parameter, given as:

$$\lambda = \begin{cases} \int_0^{\overline{\varepsilon_{\mathrm{p}}}} \dfrac{\mathrm{d}\overline{\varepsilon_{\mathrm{p}}}}{(1 + p / f_{\mathrm{t}})^{b_1}} & p \geq 0 \\ \int_0^{\overline{\varepsilon_{\mathrm{p}}}} \dfrac{\mathrm{d}\overline{\varepsilon_{\mathrm{p}}}}{(1 + p / f_{\mathrm{t}})^{b_2}} & p < 0 \end{cases} \quad (5)$$

in which f_t is the static tensile strength of concrete, $\mathrm{d}\overline{\varepsilon_{\mathrm{p}}}$ is the effective plastic strain increment, and $\mathrm{d}\overline{\varepsilon_{\mathrm{p}}} = \sqrt{(2/3)\,\mathrm{d}\varepsilon_{\mathrm{ij}}^{\mathrm{p}}\,\mathrm{d}\varepsilon_{\mathrm{ij}}^{\mathrm{p}}}$, with $\mathrm{d}\varepsilon_{\mathrm{ij}}^{\mathrm{p}}$ being the plastic strain increment tensor, η (λ) is a function of the damage parameter λ (**Fig. 5**), with $\eta(0)=0$, η (λ_m)=1, and η ($\lambda \geq \lambda_{max}$)=0; b_1 and b_2 are parameters for controlling the damage characterized from test data for compression and tension softening, respectively. This implies that the failure surface starts at the yield strength surface, and it reaches the maximum strength surface as λ increases to λ_m, and then it drops to the residual surface as λ further increases up to λ_{max}. Specific values for the λ_m, λ_{max}, and η (λ) parameters are determined from test data.

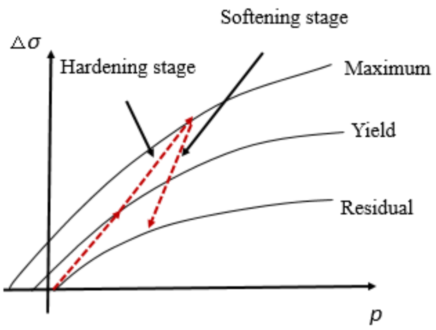

Fig. 4 Three failure surface

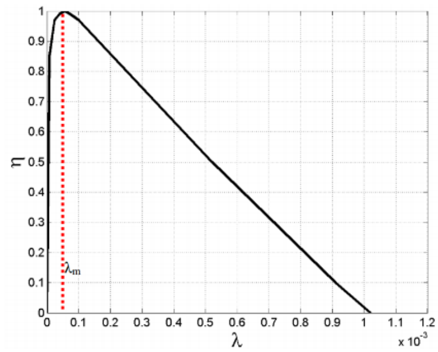

Fig. 5 Plot of η-λ curve

This model assumes a homogeneous and isotropic behavior of concrete. It can be found from **Fig. 4** that the concrete is not damaged under whatever high hydrostatic pressure. The model clearly neglects the damage to concrete material that could be induced by high hydrostatic pressure.

The automatic model parameter generation in LSDYNA version 971 is used in the simulation. The input material parameters used in the present study are listed in **Table 1**.

Table 1 Material parameters of mortar and aggregate

Parameters	Mortar	Aggregate
Density (kg/m^3)	2100	2600
Poisson's ratio	0.18	0.14
Strength (MPa)	35	90

3.2 Establishment of the 3D concrete mesoscale model

3.2.1 Generating and mapping coarse aggregates

The size of coarse aggregates considered in the mesoscale model ranges from 3.0 mm to 10 mm. The total volume percentage of aggregates is 45% according to the mixture of the concrete specimen.

Three series of course aggregates, namely 3-5, 5-8, 8-10 mm with volume percentage of 16%, 17%, 12% respectively are considered in the mesoscale model. An algorithm including two steps is implemented in FORTRAN to establish the course aggregates in the numerical model.

Step 1: Generation algorithm of coarse aggregates

Coarse aggregates are assumed to have spherical shape with random size and distribution inside the concrete specimen in the present study. The aggregate size distribution is assumed to follow Fuller's curve, which defines the grading of aggregate particles for optimum density and strength of the concrete mixture [22]. Fuller's curve is expressed by the equation

$$p(d)=100(\frac{d}{d_{\max}})^{n} \tag{6}$$

where $p(d)$ is the cumulative percentage of aggregates passing a sieve with aperture diameter d; $d_{\max}$ is the maximum size of aggregates; n is the exponent of the equation, varying from 0.45 to 0.7 and is taken as 0.5 in the present numerical study.

The procedure of generating and placing random aggregates can be summarized in the following sub-steps:

1) Random number defining the diameter of an aggregate within the size range is generated according to Fuller's curve;

2) Random coordinates for placing the aggregate within the range of the specimen are generated;

3) Whether the boundary condition is satisfied to avoid overlapping among aggregates and protruding of the aggregate outside the specimen boundary is checked;

4) If the generated aggregate satisfies the boundary conditions, record the parameters of this generation and place the aggregate in the model; otherwise delete the aggregate and perform a new generation until the boundary conditions are satisfied;

5) Repeat the above steps until all the particles are successfully placed into the concrete specimen.

Step 2: Mapping algorithm of finite element model

To generate the finite element mesh with 3D mesoscale model, the following sub-steps are implemented in FORTRAN:

1) Generate element meshes of the specimen;

2) Calculate the central coordinates of each element;

3) Generate the randomly distributed aggregates using the method in Step 1;

4) Check the position of each aggregate. If the element center locates inside one of the aggregates, assign the element with aggregate material property; otherwise fill it with mortar material property.

3.2.2 Generating and mapping pores

The pore structure of concrete is one of the most important characteristics and strongly influences its mechanical behavior. This study includes pores in the mesoscale model because pores also make concrete inhomogeneous and anisotropic, therefore affect the performance of concrete under hydrostatic pressure.

According to the references [33, 34], the pore system in cement-based materials consists of three types of pores. These are: (a) gel pores, which are micro pores of characteristic dimension 0.5-10 nm; (b) micro capillary pores (<50 nm) and macro capillaries (>50 nm to 50 μm); (3) macro pores due to entrained air and inadequate compaction with radius 50 μm to more than 2 mm. The larger the pores, the more influences they will effect on concrete properties. Considering the available computer memory and computational efficiency, only macro pores, which also affect the concrete material properties most significantly due to its size, can be modelled. In this study, 0.5 mm mesh size of hexahedral solid element is used to do this simulation. The size of pores ranging from 0.5-2 mm is considered in the simulation. The volume percentage of these pores is determined through the pore distribution on a section of the specimen. As shown in **Fig. 6**, the cross-sectional area of pores with diameters between 0.5 mm and 2 mm takes about 1.02% of the cross-sectional area of the specimen. Therefore without loss of generality the volume fraction of these pores is assumed to be 0.1% in the study. It should be noted that the volume fraction of the pores is estimated according to $(1.02\%)^{3/2}$=0.1%.

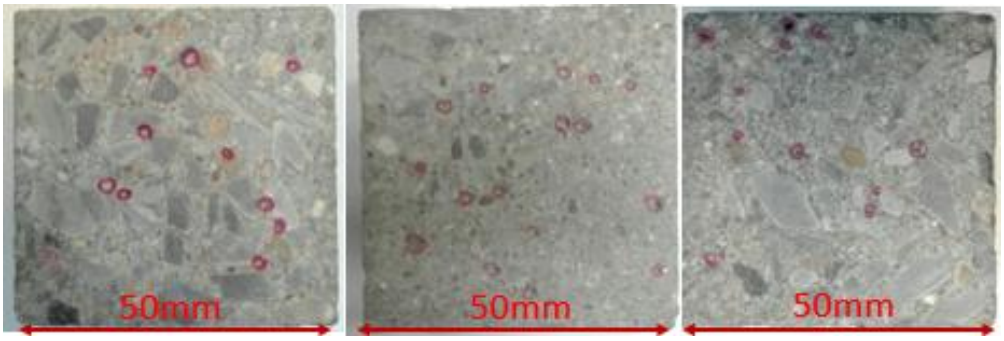

(a) (b) (c)

Fig. 6 Distribution of the pores (red circles in the photos) with diameters 0.5-2.0 mm on a cross-section of the specimen

The algorithm for generating the pores with diameter 0.5-2.0 mm in mesoscale model is similar to that of generating aggregates. The pore is randomly distributed inside the specimen and its size distribution between 0.5 mm and 2.0 mm is also assumed to follow the Fuller's curve. In this study, aggregates are generated and placed first before pores. Therefore, when generating and placing pores, the location and size of each randomly generated pore are checked to avoid pore overlapping, and also avoid overlapping with aggregates. If a generated pore locates inside one of the pores or aggregates, it is deleted and generation repeated. When a valid pore is generated, the corresponding element is deleted to generate a void in the specimen. It should be note that in the present study, the pore is simply modelled by deleting the element in the concrete specimen, i.e., modelled as a void. The air inside the pore is not considered because modelling the interaction between air and cement matrix in the specimen significantly increases the computational effort, and the influence of such interaction is believed insignificant on concrete material behavior under static loading.

3.2.3 Numerical model

It is generally agreed that ITZ is the weakest part of the micro-structural system and it plays a significant role on the mechanical properties of concrete. Micrographs of damaged concrete under hydrostatic test also confirm this point. However, the thickness of ITZ is typically 10-50 μm [30, 31, 35], modelling such thickness in a 3D mesoscale model will lead to extremely large number of elements and thus almost impossible for the current computer capacity. On the other hand, the material properties of ITZ and its transport properties between aggregates and cement paste has not been well understood [36, 37]. Therefore it is difficult to define ITZ reasonably in the simulation. This study does not model ITZ because of the above reasons, but focuses on the characteristics of stress distribution inside the concrete specimen from inhomogeneous distribution of aggregates and pores.

The dimension of the specimen is the same as those tested in the previous study [27] and the mesoscale model is shown in **Fig. 7**. The stresses along the X, Y and Z directions are perpendicularly applied on the surfaces of specimen at a rate of 10 MPa/ms (strain rate is about 0.8 1/s, according to reference [38], lateral inertial confinement effect is not prominent when the strain rate is lower than 10 1/s) to produce the hydro pressure.

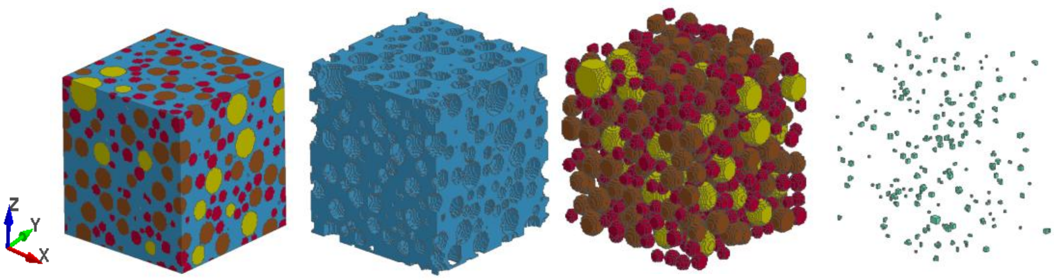

Concrete Mortar Aggregates Pores

Fig. 7 3D mesoscale model of concrete

3.3 Model validation

The established 3D mesoscale concrete model is calibrated by comparing the numerical simulation results with the test data, i.e., the stress-strain curves from the unconfined uniaxial compression test and the true tri-axial hydrostatic test. **Fig. 8** shows the stress-strain curves of experimental and numerical results of unconfined uniaxial compression. The test result and the simulation result are very similar before yielding. The numerical simulation also gives accurate prediction of concrete uniaxial strength and reflects the hardening and softening behavior of the concrete. These results validate the mesoscale concrete model using in this study. It should be noted that the concrete used in the test shows a little more plastic deformation, resulting in the strain at the maximum stress of the tested specimen is 13% larger than that of the simulation result. This modelling error could be attributed to neglecting ITZ and pores with diameter less than 0.5 mm in the model. As discussed above, ITZ is the weakest component in the specimen and it is likely to experience large plastic deformation. Similarly compaction of pores leads to large deformation. However ITZ and pores smaller than 0.5 mm are not modelled in the simulation owing to the limitation of the current computer power used in the study.

Comparison of the pressure-volumetric strain curve (equation of state) of the concrete recorded in the hydrostatic loading test and the present simulation is shown in **Fig. 9**. As can be seen, the concrete mesoscale model can reproduce the properties of EOS well, i.e., the initial elastic stage, the plastic compaction stage and fully compacted stage, indicating the reliability of the model in capturing the volumetric behavior of concrete in the loading phase. However, the mesoscale model cannot capture the unloading curve of the tested specimen accurately, i.e., unloading stiffness and a strong nonlinearity at the completion of unloading. This is because cement matrix damages when the granular skeleton, which remained elastic, recovers its initial shape. The numerical model fails to correctly simulate unloading phase because the unloading curve of the Malvar model, which is used to represent the concrete material in this study, assumes a perfect plastic deformation, i.e., the deformed aggregates could not recover its initial shape. For this reason the results of the unloading stage is not included in the following discussions. In other words the discussions are made based on the observations of specimen under tri-axial loading before unloading takes place. The numerical model can successfully simulate unloading phase only after a material model that can capture concrete material failure under hydrostatic loading is developed. The above calibrations demonstrate that, despite some inaccuracies, the developed 3D mesoscale model in general can capture the main properties of concrete specimen under uniaxial and tri-axial loading well in the loading phase, indicating the reliability of the numerical model for studying the stress distribution and damage evolution inside the concrete which cannot be recorded in hydrostatic tests.

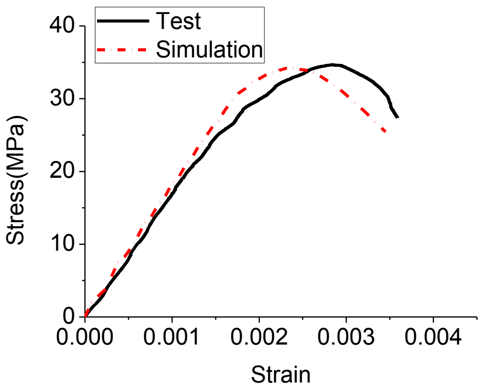

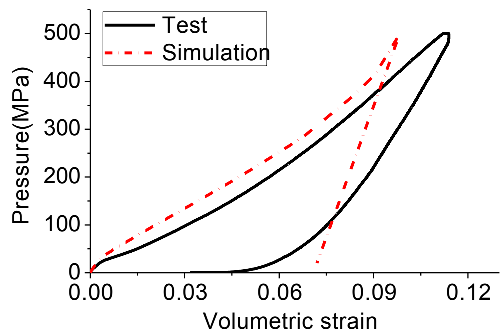

Fig. 8 Uniaxial compressive stress-strain curve **Fig. 9** Pressure-volumetric strain curve

4. Analysis of simulation results and discussion

4.1 Stress distribution inside the concrete.

Fig. 10 gives the stress distribution along X direction on an YZ-cross-section of the specimen when the volumetric strain is 0.08 (the volumetric strain is defined as the summation of strain along X, Y and Z directions of the specimen). As can be seen from the figure the stress is not evenly distributed on the cross-section, the stress in aggregates is larger than that in mortar. This is expected because the aggregates have higher bulk modulus than mortar, therefore attracts larger stress when the specimen is under hydrostatic pressure. **Fig.10 (b)** is the zoomed-in region of the red block area in the **Fig. 10 (a)**, in which element A is an element in the middle of an aggregate, element B is a mortar element connected to an aggregate, element C is a mortar element far from aggregates while element D is a mortar element close to a pore. The principal stresses σ_X (the stresses along the X direction of the specimen) of elements A, B, C and D are shown in **Fig. 11**. From the Figure, it can be found that during the loading process, the principle stresses σ_X of different elements differ a lot. The largest stress is in the aggregate element A while the lowest stress is in the mortar element D near the pore. The pore makes the mortar element around it lack of sufficient constraint to undertake high hydrostatic pressure. Therefore element D is not in a hydrostatic stress state and the deviatoric stress could damage this element although the material model used assumes the hydrostatic stress does not damage the concrete specimen.

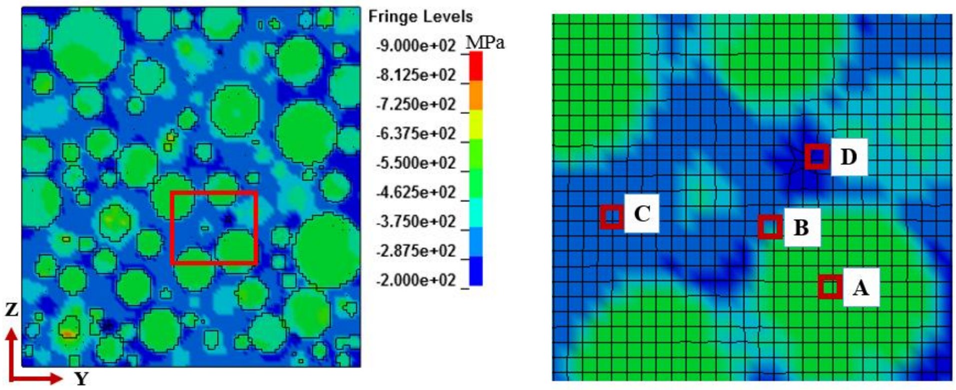

(a) (b)

Fig. 10 Stress distribution along X direction on an YZ-cross-section.

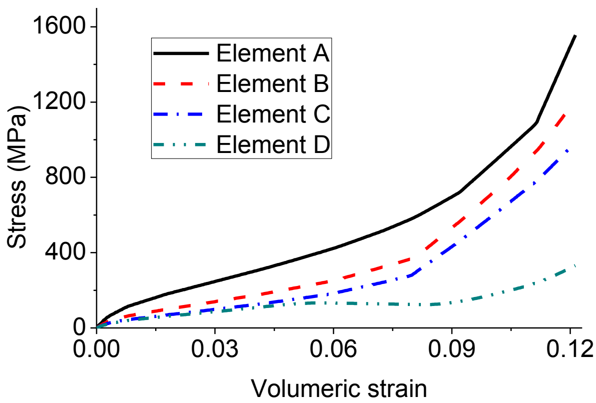

Fig. 11 The principal stresses σ_X of different elements

Figs. 12-15 show principle stresses σ_X, σ_Y and σ_Z of the four elements. One can find that the three principle stresses of element A and C are very similar while those of element B and D differ a lot. This is because the material properties of elements around A and C are the same as the material properties of elements A and C, i.e., the material of local zones of A and C can be considered as homogeneous and isotropic and so that the deviatoric stress is very small. Mortar element B is connected to the aggregate elements thus the material of its local zone is anisotropic that makes the three principle stresses very different. The boundary conditions of element D in the three principle directions are different because of the nearby pore, hence the three principle stresses are also very different. There are many other elements inside the concrete specimen subjecting to such stress conditions as element B and D which will be damaged by deviatoric stress. This is the main reason of the concrete damage under hydrostatic pressure. It should be noted that the interface between mortar and aggregates is the weakest link inside the concrete and the deviatotic stress is very obvious around these interfaces (e.g. **Fig. 13**). Therefore these interfaces are the most severely damaged region inside the concrete specimen under high hydrostatic pressure as shown in **Fig. 3**.

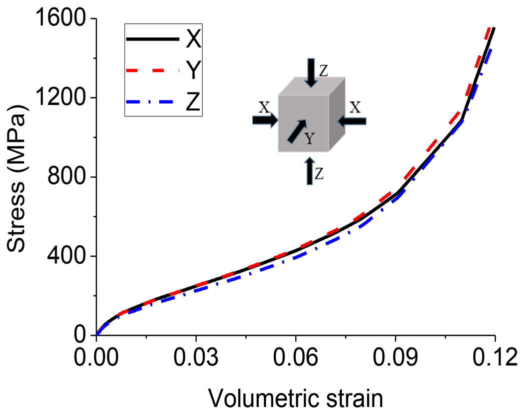

Fig. 12 Three principle stresses of element A

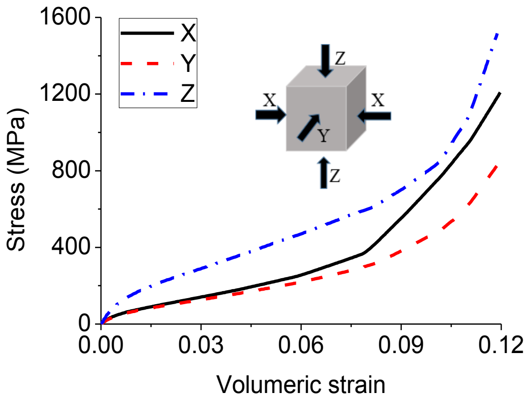

Fig. 13 Three principle stresses of element B

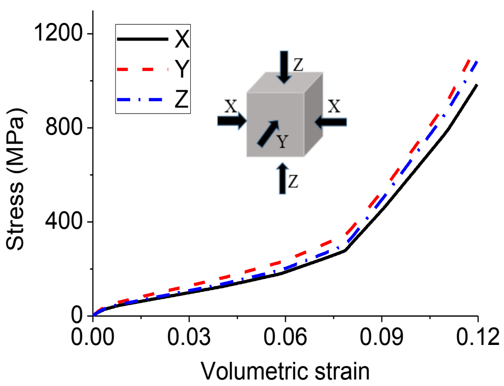

Fig. 14 Three principle stresses of element C

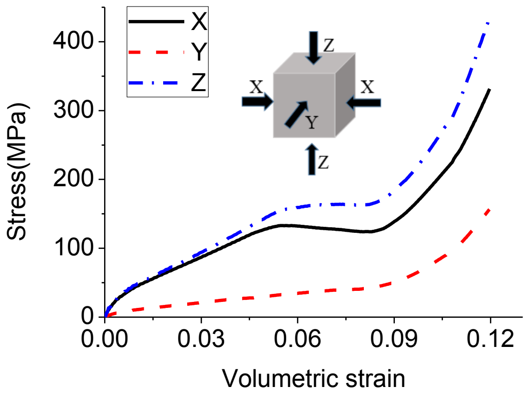

Fig. 15 Three principle stresses of element D

4.2 Damage evolution inside the concrete

Figs. 16-17 show the damage evolution of the concrete under different hydrostatic pressures. In comparison with the simulation results and experimental results, it can be noted that the simulated damage degree of the concrete is less severe than the test observations. This is because the ITZs and the pores with diameter smaller than 0.5mm are not considered in the mesoscale model. Because of the above limitations of the current numerical model, this part focuses on analyzing the damage evolution under different hydrostatic pressures and the zones where the concrete is damaged most seriously in examining the concrete specimen behavior under hydrostatic pressures. There only the damage evolution is discussed while the damage level is not considered.

It can be seen from **Fig. 16**, under 200 MPa hydrostatic pressure, the damages appear in the mortar between two closely distributed aggregates. With the increase in the hydrostatic pressure these damages are further intensified, more numbers of damages appear and some damages penetrate into the aggregates. In other words, when the applied hydrostatic pressure is very high, e.g., 1500 MPa in this example, damages are not limited to the mortar and aggregate interfaces, but distributed in wide areas of mortar matrix and can even damage aggregates. These damages can also be observed in the tests results shown in **Fig. 3 (c)**. As shown the mortar matrix between two closely spaced gravels is most seriously damaged. Other seriously damaged areas are the mortar around the pores. From **Fig. 17**, it can be found that as the hydrostatic pressure increases, the pore is compacted gradually and the damage to mortar matrix around the pore also gradually extends to a larger area. This result explains the observations reported by Karinski et al. [13] that obvious cracks were found in cement paste specimens with a higher W/C ratio which have higher porosity and larger maximum capillary pore size while no crack was observed in specimens with low W/C ratios. These damages inside the concrete specimen under hydrostatic pressure are caused because of high deviatoric stresses in these regions as shown in **Fig. 13** and **Fig. 15** owing to material heterogeneity.

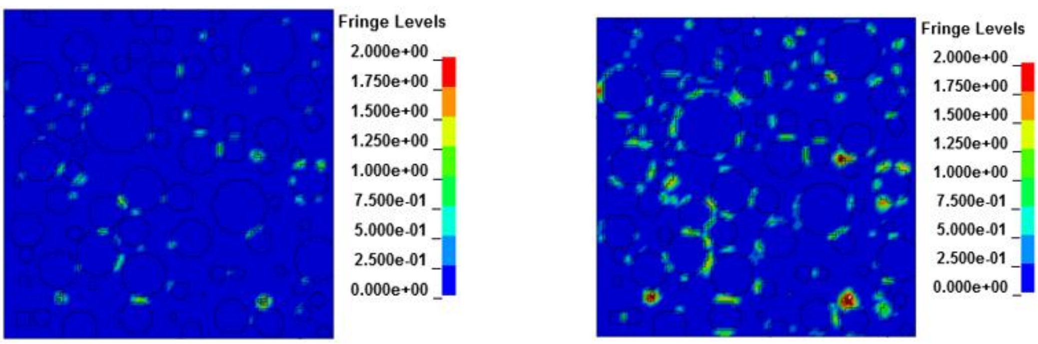

(a) 200 MPa (b) 500 MPa

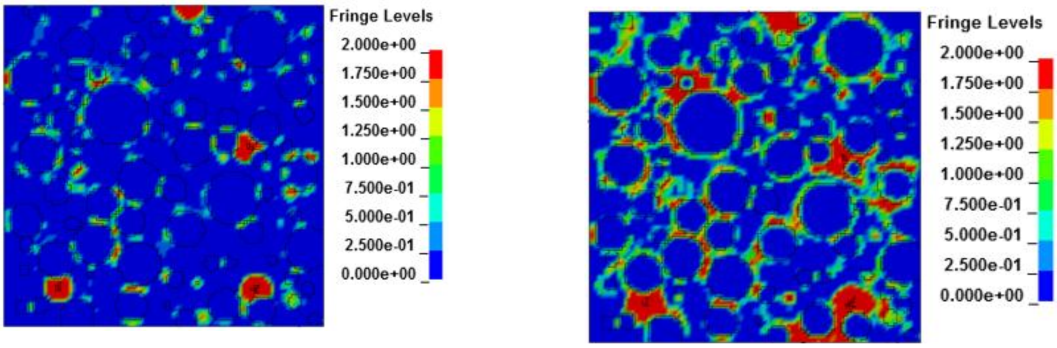

(c) 1000 MPa (d) 1500 MPa

Fig. 16 Damage evolution of concrete under different hydrostatic pressures: (a) 200 MPa; (b) 500 MPa; (c) 1000 MPa; (d) 1500 MPa

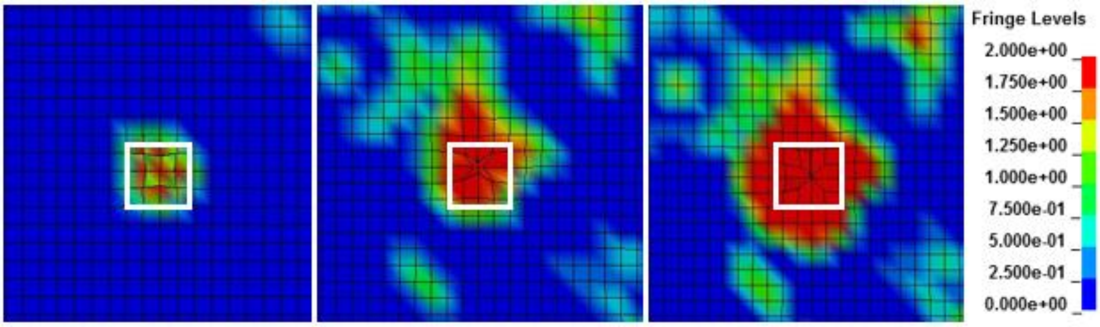

(a) 200 MPa (b) 400 MPa (c) 600 MPa

Fig. 17 Compaction of the pore and the damage evolution of the mortar around it: (a) 200 MPa; (b) 400 MPa; (c) 600 MPa

The above observations indicate that concrete material can be damaged by high-hydrostatic pressures because it is neither homogeneous nor isotropic. Unless concrete material is modelled with mesoscale or micro-scale model, which are extremely time consuming in numerical simulation and are very unlikely for general applications in modelling concrete structures, a proper concrete material model needs be developed to capture the material behavior associated with the nonhomogeneous and anisotropic properties. The current concrete material models assume the material is homogeneous and isotropic; therefore they may not capture the material behaviour under complex stress states as observed in the true tri-axial tests and in the current numerical simulations. Developing a new concrete material model, however, is beyond the scope of the current study. It could be a future research topic.

5 Conclusions

The simulation results show that the stress inside the concrete specimen is not evenly distributed under hydrostatic pressure because concrete is not a homogeneous and isotropic material, and this is the primary cause of the concrete damage under high hydrostatic pressure. ITZ and zones around pores are the most vulnerable areas because the deviatoric stresses are developed in these areas and damage the material. Mortar between closely distributed aggregates is the most vulnerable because of the strong material heterogeneity in these areas and possible stress concentrations. Current concrete material models cannot capture these damages and material behavior under hydrostatic pressures because they assume concrete as a homogeneous and isotropic material.

6 Acknowledgments

The authors gratefully acknowledge the support from China National Nature Science Foundation [51378346], and the Australian Research Council [DP160104557] for carrying out this research.

7 References

[1] Y. Karinski, S. Zhutovsky, V. Feldgun, D. Yankelevsky, The equation of state of unsaturated cementitious composites–A new multiscale model, International Journal of Solids and Structures 109 (2017) 12-21.

[2] M. Petkovski, Experimental detection of damage evolution in concrete under multiaxial compression, Journal of Engineering Mechanics 139(5) (2012) 616-628.

[3] F. Ansari, Q. Li, High-strength concrete subjected to triaxial compression, ACI Materials Journal 95 (1998) 747-755.

[4] D. Candappa, J. Sanjayan, S. Setunge, Complete triaxial stress-strain curves of high-strength concrete, Journal of Materials in Civil Engineering 13(3) (2001) 209-215.

[5] K.A. Harries, G. Kharel, Experimental investigation of the behavior of variably confined concrete, Cement and Concrete Research 33(6) (2003) 873-880.

[6] X.H. Vu, Y. Malecot, L. Daudeville, E. Buzaud, Experimental analysis of concrete behavior under high confinement: Effect of the saturation ratio, International Journal of Solids and Structures 46(5) (2009) 1105-1120.

[7] L.J. Malvar, J.E. Crawford, J.W. Wesevich, D. Simons, A plasticity concrete material model for DYNA3D, International Journal of Impact Engineering 19(9-10) (1997) 847-873.
[8] W. Riedel, K. Thoma, S. Hiermaier, E. Schmolinske, Penetration of reinforced concrete by BETA-B-500 numerical analysis using a new macroscopic concrete model for hydrocodes, Proceedings of the 9th International Symposium on the Effects of Munitions with Structures, sn, 1999.
[9] LS-DYNA version ls971 R7.0.0, Livermore Software Technology Corporation. Livermore, CA.
[10] J. Cui, H. Hao, Y. Shi, Discussion on the suitability of concrete constitutive models for high-rate response predictions of RC structures, International Journal of Impact Engineering 106 (2017) 202-216.
[11] C. Poinard, Y. Malecot, L. Daudeville, Damage of concrete in a very high stress state: experimental investigation, Materials and Structures 43(1-2) (2010) 15-29.
[12] T.M. Pham, M.N. Hadi, T.M. Tran, Maximum usable strain of FRP-confined concrete, Construction and Building Materials 83 (2015) 119-127.
[13] Y. Karinski, D. Yankelevsky, S. Zhutovsky, V. Feldgun, Uniaxial confined compression tests of cementitious materials, Construction and Building Materials 153 (2017) 247-260.
[14] Z. Agioutantis, C. Stiakakis, S. Kleftakis, Numerical simulation of the mechanical behaviour of epoxy based mortars under compressive loads, Computers & structures 80(27) (2002) 2071-2084.
[15] Y. Huang, Z. Yang, X. Chen, G. Liu, Monte Carlo simulations of meso-scale dynamic compressive behavior of concrete based on X-ray computed tomography images, International Journal of Impact Engineering 97 (2016) 102-115.
[16] N. Tregger, D. Corr, L. Graham-Brady, S. Shah, Modeling the effect of mesoscale randomness on concrete fracture, Probabilistic engineering mechanics 21(3) (2006) 217-225.
[17] Z. Wang, A. Kwan, H. Chan, Mesoscopic study of concrete I: generation of random aggregate structure and finite element mesh, Computers & Structures 70(5) (1999) 533-544.
[18] X. Zhou, H. Hao, Mesoscale modelling of concrete tensile failure mechanism at high strain rates, Computers & Structures 86(21) (2008) 2013-2026.
[19] S. Häfner, S. Eckardt, T. Luther, C. Könke, Mesoscale modeling of concrete: Geometry and numerics, Computers & structures 84(7) (2006) 450-461.
[20] S.M. Kim, R.K.A. Al-Rub, Meso-scale computational modeling of the plastic-damage response of cementitious composites, Cement and Concrete Research 41(3) (2011) 339-358.
[21] X. Wang, Z. Yang, J. Yates, A. Jivkov, C. Zhang, Monte Carlo simulations of mesoscale fracture modelling of concrete with random aggregates and pores, Construction and Building Materials 75 (2015) 35-45.

[22] P. Wriggers, S. Moftah, Mesoscale models for concrete: Homogenisation and damage behaviour, Finite elements in analysis and design 42(7) (2006) 623-636.
[23] G. Chen, Y. Hao, H. Hao, 3D meso-scale modelling of concrete material in spall tests, Materials and Structures 48(6) (2015) 1887.
[24] B. Erzar, P. Forquin, Experiments and mesoscopic modelling of dynamic testing of concrete, Mechanics of Materials 43(9) (2011) 505-527.
[25] N.S. Martys, C.F. Ferraris, Capillary transport in mortars and concrete, Cement and Concrete Research 27(5) (1997) 747-760.
[26] I. Yaman, N. Hearn, H. Aktan, Active and non-active porosity in concrete part I: experimental evidence, Materials and Structures 35(2) (2002) 102.
[27] J. Cui, H. Hao, Y. Shi, X. Li, K. Du, Experimental study of concrete damage under high hydrostatic pressure, Cement and Concrete Research 100 (2017) 140-152.
[28] K. Du, M. Tao, X.-b. Li, J. Zhou, Experimental Study of Slabbing and Rockburst Induced by True-Triaxial Unloading and Local Dynamic Disturbance, Rock Mechanics and Rock Engineering 49(9) (2016) 3437-3453.
[29] X. Li, K. Du, D. Li, True triaxial strength and failure modes of cubic rock specimens with unloading the minor principal stress, Rock Mechanics and Rock Engineering 48(6) (2015) 2185-2196.
[30] W.A. Tasong, C.J. Lynsdale, J.C. Cripps, Aggregate-cement paste interface: Part I. Influence of aggregate geochemistry, Cement and Concrete Research 29(7) (1999) 1019-1025.
[31] J. Xiao, W. Li, D.J. Corr, S.P. Shah, Effects of interfacial transition zones on the stress–strain behavior of modeled recycled aggregate concrete, Cement and Concrete Research 52 (2013) 82-99.
[32] W.F. Chen, Plasticity in reinforced concrete, J. Ross Publishing 2007.
[33] R. Kumar, B. Bhattacharjee, Porosity, pore size distribution and in situ strength of concrete, Cement and concrete research 33(1) (2003) 155-164.
[34] E.K. Nambiar, K. Ramamurthy, Air-void characterisation of foam concrete, Cement and concrete research 37(2) (2007) 221-230.
[35] K.L. Scrivener, A.K. Crumbie, P. Laugesen, The interfacial transition zone (ITZ) between cement paste and aggregate in concrete, Interface Science 12(4) (2004) 411-421.
[36] A. Bentur, M. Alexander, A review of the work of the RILEM TC 159-ETC: Engineering of the interfacial transition zone in cementitious composites, Materials and structures 33(2) (2000) 82-87.
[37] S. Erdem, A.R. Dawson, N.H. Thom, Influence of the micro-and nanoscale local mechanical properties of the interfacial transition zone on impact behavior of concrete made with different aggregates, Cement and Concrete Research 42(2) (2012) 447-458.

[38] Y. Hao, H. Hao, Z.X. Li, Numerical analysis of lateral inertial confinement effects on impact test of concrete compressive material properties, International Journal of Protective Structures 1(1) (2010) 145-167.